RESEARCH ARTICLE

NANO · MICRO small
www.small-journal.com

Highly Ionic Conductive, Stretchable, and Tough Ionogel for Flexible Solid-State Supercapacitor

Ying Wang, Zhengxuan Wei, Tongtai Ji, Ruobing Bai, and Hongli Zhu**

The increasing demand for wearable electronics calls for advanced energy storage solutions that integrate high electrochemical performances and mechanical robustness. Ionogel is a promising candidate due to its stretchability combined with high ionic conductivity. However, simultaneously optimizing both the electrochemical and mechanical performance of ionogels remains a challenge. This paper reports a tough and highly ion-conductive ionogel through ion impregnation and solvent exchange. The fabricated ionogel consists of double interpenetrating networks of long polymer chains that provide high stretchability. The polymer chains are crosslinked by hydrogen bonds that induce large energy dissipation for enhanced toughness. The resultant ionogel possesses mechanical stretchability of 26, tensile strength of 1.34 MPa, and fracture toughness of 4175 J m^{-2}. Meanwhile, due to the high ion concentrations and ion mobility in the gel, a high ionic conductivity of 3.18 S m^{-1} at room temperature is achieved. A supercapacitor of this ionogel sandwiched with porous fiber electrodes provides remarkable areal capacitance (615 mF cm^{-2} at 1 mA cm^{-2}), energy density (341.7 µWh cm^{-2} at 1 mA cm^{-2}), and power density (20 mW cm^{-2} at 10 mA cm^{-2}), offering significant advantages in applications where high efficiency, compact size, and rapid energy delivery are crucial, such as flexible and wearable electronics.

1. Introduction

The extensive demand and rapid development of wearable electronics bring growing requirements for their supporting energy storage units. To support a wearable electronic device, its energy storage unit, such as a battery or supercapacitor, needs excellent electrochemical performances (e.g., ionic conductivity and electrochemical stability window, ESW) to ensure the electrical functionality, robust mechanical properties (e.g., flexibility, stretchability, strength, and toughness) to sustain mechanical loads in various working conditions, and reliable safety to avoid fire or hazardous leaking due to electrical breakdown or mechanical failures.[1]

Y. Wang, Z. Wei, T. Ji, R. Bai, H. Zhu
Department of Mechanical and Industrial Engineering
Northeastern University
Boston, MA 02115, USA
E-mail: ru.bai@northeastern.edu; h.zhu@neu.edu

The ORCID identification number(s) for the author(s) of this article can be found under https://doi.org/10.1002/smll.202307019

DOI: 10.1002/smll.202307019

Compared to conventional liquid-state electrolytes, gel polymer electrolytes (GPEs) hold great promise for addressing multifaceted challenges from mechanics and general safety.[2,3] A GPE is composed of a polymer network in a mixture with an alkali metal salt solution. The polymer network provides solid-like mechanical properties, while the salt solution provides adequate ion transfer.[4,5] One typical example is the widely studied ionically conductive hydrogel made of hydrophilic polymer networks and aqueous ion solution. These ionic hydrogels have been developed in recent years with superior mechanical properties (stretchability of > 10 times its original length, strength over 1.0 MPa, and fracture toughness > 10^4 J m^{-2}) and sufficient ionic conductivity (as high as > 1.0 S m^{-1}).[6–8] However, a large amount of water solvent (> 60 wt%) in these hydrogels limits their electrochemical stability windows (ESWs) to ≈1.0 V, if no special functionalization or modification of polymer chains is introduced,[9] together with poor physical stability due to water evaporation[10] and reduced low-temperature performance because of water freezing.[11]

By far, *ionogel* replaces water with an ionic liquid as its solvent, leading to enhanced ESW (above 1.0 V) while maintaining a satisfying ionic conductivity (as high as 2.5 S m^{-1}).[12,13] In addition, most ionic liquids have low vapor pressures, making them nearly non-volatile in an ambient environment. Because of these advantages, developments of new ionogels as electrolytes have drawn growing attention in recent years. However, an ionogel with both excellent electrochemical performance and robust mechanical properties has remained challenging. Ionogels with ionic conductivity comparable to their corresponding pure ionic liquids (on the order of 1.0 S m^{-1} at room temperature) have been developed but with weaker mechanical properties compared to many state-of-the-art hydrogels (e.g., a fracture stretch of ≈3.5 times of an ionogel compared to > 10 times of many hydrogels).[14–16] On the other hand, P(Aam-co-AA)-EMIES, PEO-Li^+-PEO-PPO-PEO-BMImTFSI, and P(AA-co-VI)-BMImCl ionogels with superior mechanical properties (e.g., strength > 1 MPa and fracture toughness > 4000 J m^{-2}) have also been developed,[17–19] but their ionic conductivities are mostly < 0.5 S m^{-1} that is far away the corresponding ionic liquids, greatly limiting their capabilities as electrolytes.

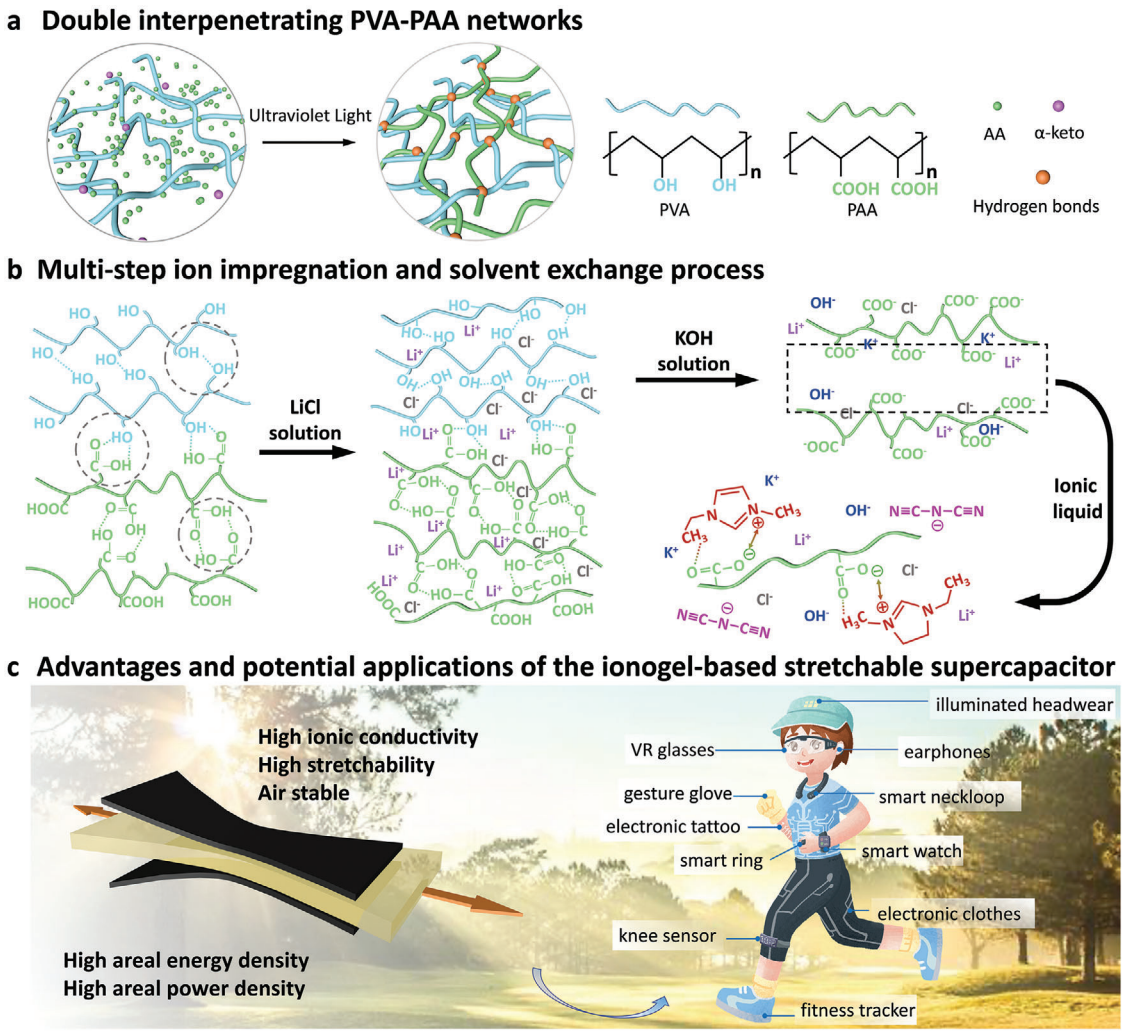

Figure 1. a) The synthesis and molecular structure of the PVA-PAA hydrogel. b) The subsequent multi-step ion impregnation and solvent exchange process toward the final PVA-PAA-LiCl-KOH ionogel. c) Advantages and potential applications of the ionogel-based stretchable supercapacitor.

Here, we developed a new ionogel with excellent ionic conductivity, electrochemical stability window, mechanical property, and physical stability through ion impregnation and solvent exchange. We first synthesized a host hydrogel with interpenetrating polymer networks. Then, we modified these networks via ion impregnation. Afterward, we replaced the water solvent with a highly conductive ionic liquid in the gel through solvent exchange process. We characterized the ionic conductivity, electrochemical stability window, mechanical stretchability, strength, fracture toughness, and long-term stability at an ambient temperature of the fabricated ionogel. The ionogel maintains a small amount of residual water, which assists the highly concentrated ions to enable facile migration and provide high ionic conductivity over a wide temperature range. Despite this residual water, the ionogel exhibits a remarkably wide electrochemical stability window of 2.0 V, far surpassing hydrogels. Concurrently, the developed networks and co-functioning ions render this ionogel with remarkable and tough mechanical performances. The ionogel further exhibits excellent physical stability in weight and ionic conductivity over 40 h at an ambient temperature and low relative humidity of 20%. Finally, we sandwiched the ionogel with high surface area polyacrylonitrile-derived porous carbon fibers (PPCF) electrodes to create a flexible supercapacitor with superior areal capacitance, energy, and power densities compared to most existing gel-based solid-state supercapacitors.

2. Results and Discussion

To fabricate the ionogel, an ion impregnation and solvent exchange method is designed. Acrylic acid (AA) monomers were in situ polymerized with polyvinyl alcohol (PVA) polymer chains in an aqueous solution following a free-radical polymerization without any covalent crosslinker. The synthesized PAA-PVA hydrogel has interpenetrating networks crosslinked by hydrogen bonds between the abundant hydroxyl groups (—OH) on the PVA and the carboxyl groups (—COOH) on the PAA (**Figure 1a**). Afterward, the PVA-PAA hydrogel was immersed in a LiCl solution with a prescribed high concentration. This induces a salting-out effect on the hydrogel (Figure 1b), which greatly

increases the number of hydrogen bonds formed between polymer chains.[20,21] The resulting PVA-PAA-LiCl hydrogel was subsequently immersed in a KOH solution to transform the neutral PAA chains to charged polyelectrolytes with —COO^- groups, which re-swells the hydrogel due to electrostatic repulsion between chains and osmotic pressures from mobile ions.[22] Finally, the re-swollen PVA-PAA-LiCl-KOH hydrogel was freeze-dried to remove the free water while retaining the expanded polymer structure and then immersed in the 1-ethyl-3-methylimidazolium dicyanamide ([EMIm][DCA]) ionic liquid to form the target PVA-PAA-LiCl-KOH ionogel.

This design with multi-step fabrication brings combined advantages to both the electrochemical performance and mechanical properties of the ionogel. The deliberately chosen [EMIm][DCA] possesses the highest ionic conductivity among existing ionic liquids, 2.8 S m^{-1}, at room temperature.[14] The ionic liquid is effectively encapsulated by the polymer networks through ionic complexation between itself and the deprotonated PAA chains.[17] Throughout the synthesis, a trace amount of water stays in the ionogel (to be discussed in detail later), which further enhances the ionic conductivity without adversely affecting the ESW.[23] Simultaneously, the substantial hydrogen bonds in the ionogel induce high energy dissipation during large deformation or crack propagation via a large volume of bond breaking.[24] The long PAA and PVA chains with no additional covalent crosslinker provide high mechanical stretchability. The synergy of the high energy dissipation and long polymer chains leads to both high strength and fracture toughness.[25] With these outstanding electrochemical and mechanical properties, as will be shown, the non-volatile ionic liquid further ensures superior physical stability in weight and ionic conductivity compared to existing hydrogels. Therefore, a packaging-free solid-state supercapacitor made of this ionogel is expected to simplify the process and reduce the cost of production, as well as to be commercialized through a mass market launch toward broad applications of portable and wearable smart devices (Figure 1c).

The evolution of the molecular structure and free water content in the gel throughout the multi-step fabrication was investigated in **Figure 2**a using scanning electron microscopy (SEM). The PVA-PAA hydrogel is initially transparent (Figure 2a1), with nearly homogeneous honeycomb-like microscopic pores in the dry state (Figure 2a2). After the LiCl treatment, the polymer chains condense, and the gel de-swells due to the additional crosslinking by hydrogen bonds (Figure 2a3),[20,26] leading to a much more compact structure with thicker walls in the SEM image (Figure 2a4). Immersing the gel in the KOH solution considerably re-swells the polymer networks and hydrogel (Figure 2a5). Meanwhile, the thick-wall microstructure is retained with significantly expanded pores (Figure 2a6) compared to the initial PVA-PAA hydrogel. This alkali (KOH) treatment of the gel network is highly necessary to facilitate the permeation of ionic liquids into the network. As control experiments, excluding this treatment (Figure S1, Supporting Information) or replacing KOH with water (Figures S2,S3, Supporting Information) greatly changes the final structure and performances of the ionogel. Finally, after freeze-drying and soaking in the ionic liquid, the polymer microstructure is slightly tightened again (Figure 2a7,8). The color of the gel changes from translucent to light yellow, indicating the successful retaining of the ionic liquid.

To detailly understand the chemical structures of gels during each fabrication step, functional groups of the PVA-PAA, PVA-PAA-LiCl, PVA-PAA-LiCl-KOH hydrogels, as well as the PVA-PAA-LiCl-KOH ionogel, were characterized utilizing the Fourier-transform infrared spectroscopy (FTIR). As presented in Figure 2b, all samples display characteristic peaks at 3430 and 1641 cm^{-1} corresponding to the stretching vibration of the —OH and at 1432 cm^{-1} to the asymmetric stretching vibration of the —COOH group.[27] In the PVA-PAA-LiCl-KOH hydrogel, the blue shift of the O—H stretching peak around 3430 cm^{-1} (black arrow in Figure 2b) indicates the decreasing density of hydrogen bonds. Moreover, the peaks of stretching vibrations of C═O and C—O from PAA at 1706 and 1260 cm^{-1} become much weaker,[28] suggesting weaker physical interactions due to the re-swelling of PAA chains. In the PVA-PAA-LiCl-KOH ionogel, the peaks at 1260 cm^{-1} reappear, demonstrating denser PAA chains. The emergence of the peak at 1563 cm^{-1} in the PVA-PAA-LiCl-KOH hydrogel and the ionogel corresponds to the asymmetric stretching vibration absorption of C═O resulting from the —COOH group interacting with KOH (Figure S4, Supporting Information).[29] Finally, the ionogel exhibits peaks at 2200 and 2190 cm^{-1}, attributed to the stretching vibration of C≡N. The stronger bond signal at 1563 cm^{-1} corresponds to the N—H vibration in the ionic liquid (Figure S5, Supporting Information). These peak signals again prove the successful incorporation of the ionic liquid into the gel.

The thermal stability of different gels was studied by thermogravimetric analysis (TGA) and derivative thermogravimetry (DTG) in Figure 2c and Figure S6 (Supporting Information), respectively. In the TGA tests, the first weight loss of gels below 100 °C results from the evaporation of free water. The amount of free water content in each gel is consistent with the observed swelling ratio and microstructure, as previously discussed. Calculated from the TGA data, the final ionogel exhibits a water content of 6.7 wt%, much lower than that of the pristine PVA-PAA hydrogel, 21.8 wt%. For the PVA-PAA and PVA-PAA-LiCl hydrogels, second and third weight losses are observed at ≈300 °C and above 400 °C, corresponding to the evaporation of bonded water and the degradation of polymer chains, respectively. For the PVA-PAA-LiCl-KOH hydrogel, the TGA curve is nearly flat at a temperature above 150 °C, possibly due to the reduced interaction between polymer chains caused by the large swelling.[30] For the PVA-PAA-LiCl-KOH ionogel, only a loss temperature at 460 °C is observed after the initial free-water evaporation, corresponding to the thermal decomposition of the ionic liquid. This loss temperature is higher than the decomposition temperature of the pure ionic liquid at 310 °C (Figure S7, Supporting Information), suggesting the good interaction between the ionic liquid and polymer chains.

Figure 3a shows uniaxial tensile stress–stretch curves of various hydrogels up to fracture. In each curve, we define the peak as the tensile strength of the gel and the ultimate fracture stretch as the stretchability. Compared to the pristine PVA-PAA hydrogel, the PVA-PAA-LiCl hydrogel shows significantly enhanced strength from ≈0.25 to 2.1 MPa, while maintaining a high stretchability of ≈8. To investigate the effect of LiCl, gels treated with 6 and 8 M LiCl solutions are characterized. No distinctive difference is observed between their stress-stretch curves, possibly due to the high enough concentrations of LiCl in both cases.

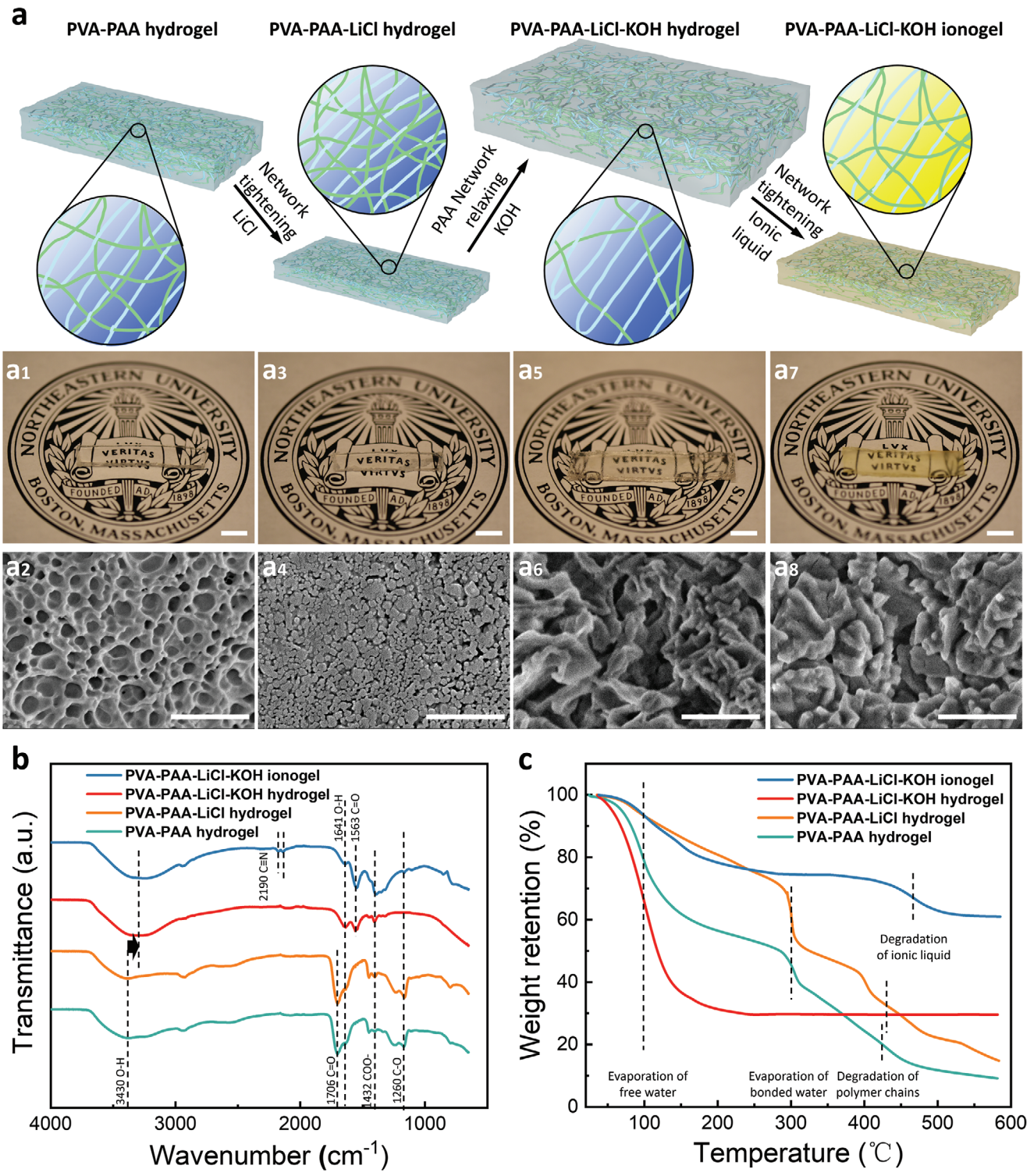

Figure 2. Characterizations of gels throughout the multi-step fabrication. a) Schematics, photos, and scanning electron microscopy (SEM) images of the PVA-PAA (a1,2), PVA-PAA-LiCl (a3,4), PVA-PAA-LiCl-KOH (a5,6) hydrogels, and the PVA-PAA-LiCl-KOH ionogel (a7,8). b) Fourier-transform infrared spectroscopy and c) thermogravimetric analysis results of the four gels. The scale bars are 1.0 cm in the photos and 1.0 μm in the SEM images.

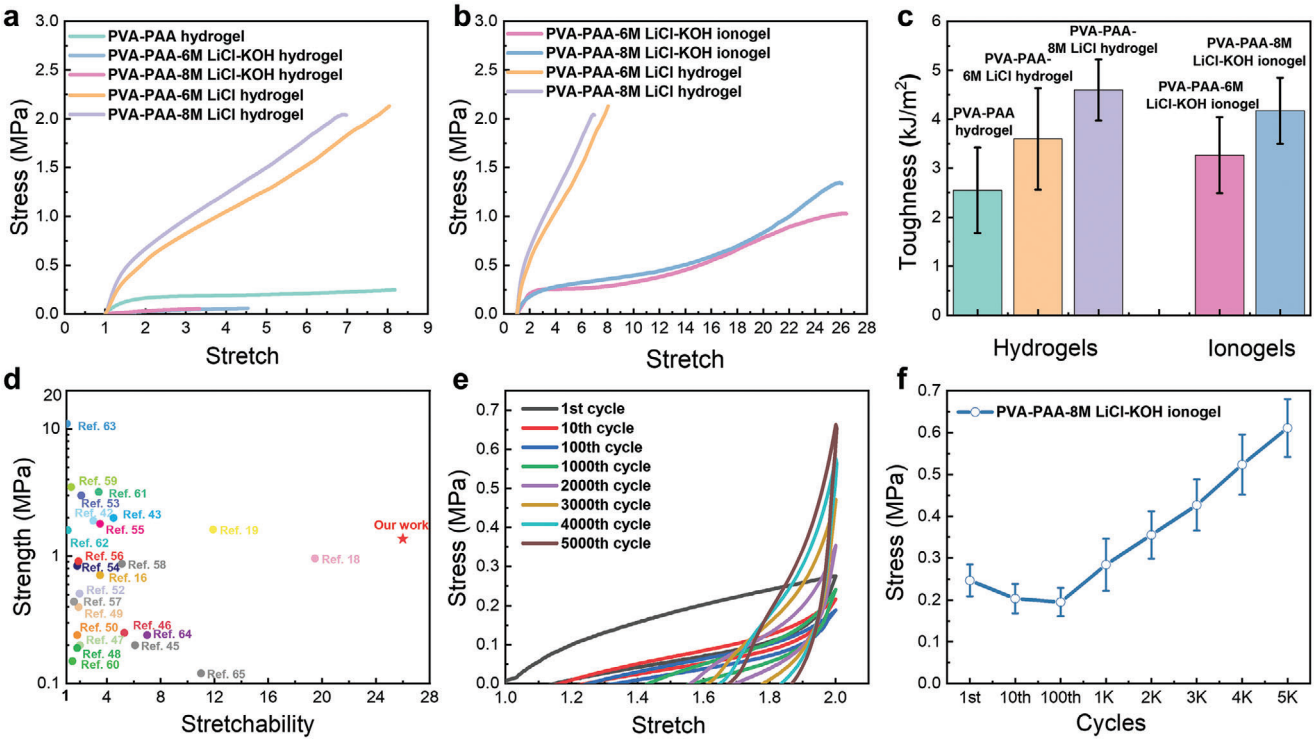

Figure 3. Mechanical characterizations of different gels. a-b) Uniaxial tensile stress–stretch curves and c) fracture toughness of different hydrogels and ionogels. d) Ashby plot on the stretchability and fracture strength among all reported ionogels.[16,18,19,42–65] e) Cyclic stress–stretch curves of an uncut ionogel with a stretch amplitude of 2 . f) The maximum stress over cycles from (e).

In addition, the PVA-PAA-LiCl-KOH hydrogel shows much reduced strength (< 0.1 MPa) and stretchability (< 4), consistent with the much larger swelling of its polymer networks, as shown by the photos and SEM images in Figure 2a.

Figure 3b compares the PVA-PAA-LiCl-KOH ionogels with the PVA-PAA-LiCl hydrogels from Figure 3a. After the solvent exchange, the stretchability of the ionogel dramatically increases from 7 to 26, with a modest decrease of strength to ≈1.34 MPa (Figure 3b). This is likely a consequence of several coupling factors in the ionogel, including the reduced number of hydrogen bonds (as cross-links and sacrificial bonds, which enhance the strength and toughness, but reduce the stretchability),[24,31,32] a much higher solvent content (which reduces the strength and toughness but greatly enhances the stretchability),[33,34] and larger pores after freeze-drying (which possibly enhance the stretchability).

The fracture toughness of various gels was measured using the well-established edge-crack test (Figure S8, Supporting Information).[35] As shown in Figure 3c, all the gels (except the PVA-PAA-LiCl-KOH hydrogel that is brittle and not characterized) exhibit high fracture toughness in the range of 2000–5000 J m^{-2}. In particular, the ionogel shows a fracture toughness as high as ≈4000 J m^{-2}, slightly depending on the concentration of LiCl. The high fracture toughness on the order of 10^3 J m^{-2} is comparable to the state-of-the-art tough hydrogels that have been widely reported.[25] Due to a general lack of reported data on the fracture toughness of ionogels, we construct an Ashby plot to compare the stretchability and fracture strength instead of all reported ionogels in the literature (Figure 3d). Our material outperforms most existing ionogels with a strength of over 1 MPa and shows the highest stretchability of ≈26.

The fatigue behavior of the PVA-PAA ionogel was characterized by conducting uniaxial cyclic mechanical loads of an uncut sample with a stretch amplitude of 2 for 5000 cycles (Figure 3e), together with the maximum stress in each cycle (Figure 3f). Over cyclic loads, the stress–stretch curves show an initial softening with a decrease of the maximum stress (e.g., 1st, 10th, and 100th in Figure 3e,f), followed by a significant stiffening and strengthening. Based on previous studies on tough hydrogels and PVA hydrogels,[21,24,36,37] we attribute the initial cyclic softening to the accumulated internal damage of the polymer network due to the hydrogen bond breaking. Over 100 cycles, the reversible hydrogen bonds gradually reform along the stretching direction of the polymer chains, leading to increasing sample length, stiffness, and maximum stress.[24,38] This indicates that the dense and reversible hydrogen bonds make the ionogel resistant to fatigue damage, that is, the continuous softening of the stretch–stretch response over accumulated cyclic loads.[39] This further suggests that the current ionogel will be highly resistant to fatigue fracture, that is, the continuous crack propagation over cyclic loads, which has been demonstrated recently by other similar anti-fatigue-fracture gels formed by PVA networks with dense hydrogen bonds.[40,41]

Not only in terms of mechanical properties, the incorporation of supplementary ions and the resulting alteration of the microstructure of the polymer network have a significant impact on the ionic conductivity of ionogels. In brief, the introduction of significant quantities of Li^+ and Cl^- enhances the

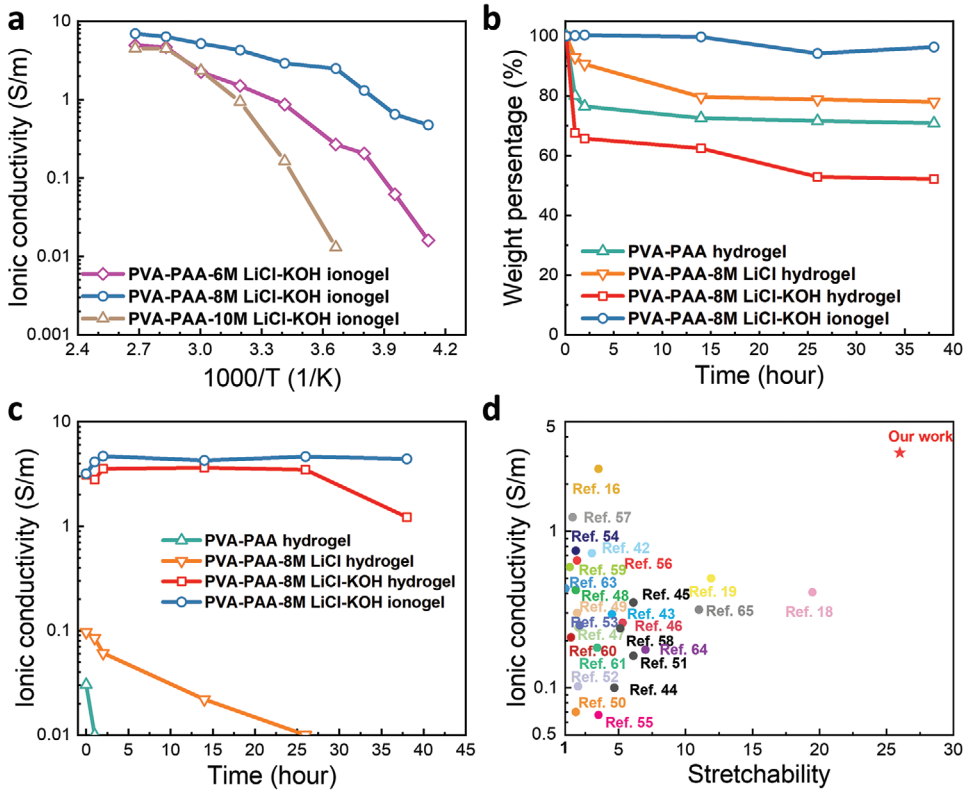

Figure 4. a) Plot of ionic conductivity at different temperatures. Physical stability of different gels. b) The change of weight and c) the ionic conductivity of gels over time at the ambient temperature with a relative humidity of 20%. d) Ashby plot on the ionic conductivity and stretchability among all reported ionogels.[16,18,19,42–65]

concentration of ions and enhances the ionic conductivity of gels. However, this increase in ion concentration also leads to the contraction of the networks, which in turn hinders the mobility of ions during impregnation. Unlike LiCl, the KOH solvent immersion process can enhance ionic conductivity through both more ions introduction and swelled networks. Through a series of complex processes and mechanisms, the ionogel treated with 8 M LiCl exhibited superior ionic conductivity than those treated with 6 and 10 M LiCl. Further elucidation of the collaborative influence of additional ions (Li^+, Cl^-, K^+, and OH^-), water, and ionic liquid on the ionic conductivity of gels is observed and expounded in Figures S9–S12 (Supporting Information).

The above effects are consistent across temperatures. Arrhenius plot, **Figure 4a**, shows the temperature effect of the ionic conductivity in ionogels with various concentrations of LiCl. The ionogel treated with 8 M LiCl shows the highest ion transfer kinetic and the best ionic conductivity with a decrease by only one order of magnitude from room temperature (3.18 S m^{-1}) to −30 °C (0.48 S m^{-1}), at which the ionic liquid [EMIm][DCA] crystallizes.[68] This ionic conductivity outperforms other existing anti-freezing gels by about one order of magnitude over a wide range of temperatures (Figure S13, Supporting Information).[60,69–75] The high ionic conductivity at low temperatures highlights the potential of this ionogel for applications in extreme environments.

Superior to its precursor, this ionogel demonstrates both high ionic conductivity and adequate physical and electrochemical stability. The weight stability of gels is contingent upon their solvent vapor pressures and content, as well as the level of porosity inherent in their network architecture. Increasing water content and a looser network structure lead to faster water loss and weight instability. The ionogel shows excellent physical stability over long-time exposure in an ambient temperature. To demonstrate, different hydrogels and ionogels were placed to an environment with a room temperature of 25 °C and relative humidity (RH) of 20%, with their weights recorded over time (Figure 4b). After ≈40 h, the ionogel retains a fraction of 96% of its initial weight. By contrast, all hydrogels lose a considerable amount of water within the first hour (80%, 93%, and 68% for the PVA-PAA, PVA-PAA-LiCl, and PVA-PAA-LiCl-KOH hydrogels, respectively).

The physical stability of the ionogel is further reflected by its remarkably stable ionic conductivity measured over time (Figure 4c). The ionic conductivity of ionogel slightly increases for the initial 3 h at the ambient environment and then maintains constant over 40 h. Additionally, the ionogel exhibits outstanding stability in the elongated period of 100 h at ambient temperature, as shown in Figure S14 (Supporting Information). By contrast, the ionic conductivity of a PVA-PAA hydrogel dramatically decreases to a vanishingly low value within 2 h. The ionic conductivity of a PVA-PAA-LiCl hydrogel shows a slower decrease than its precursor over time and close to 0.01 S m^{-1} after 25 h. The ionic conductivity of a PVA-PAA-LiCl-KOH hydrogel is more stable compared to other hydrogels but still starts to decrease after 25 h.

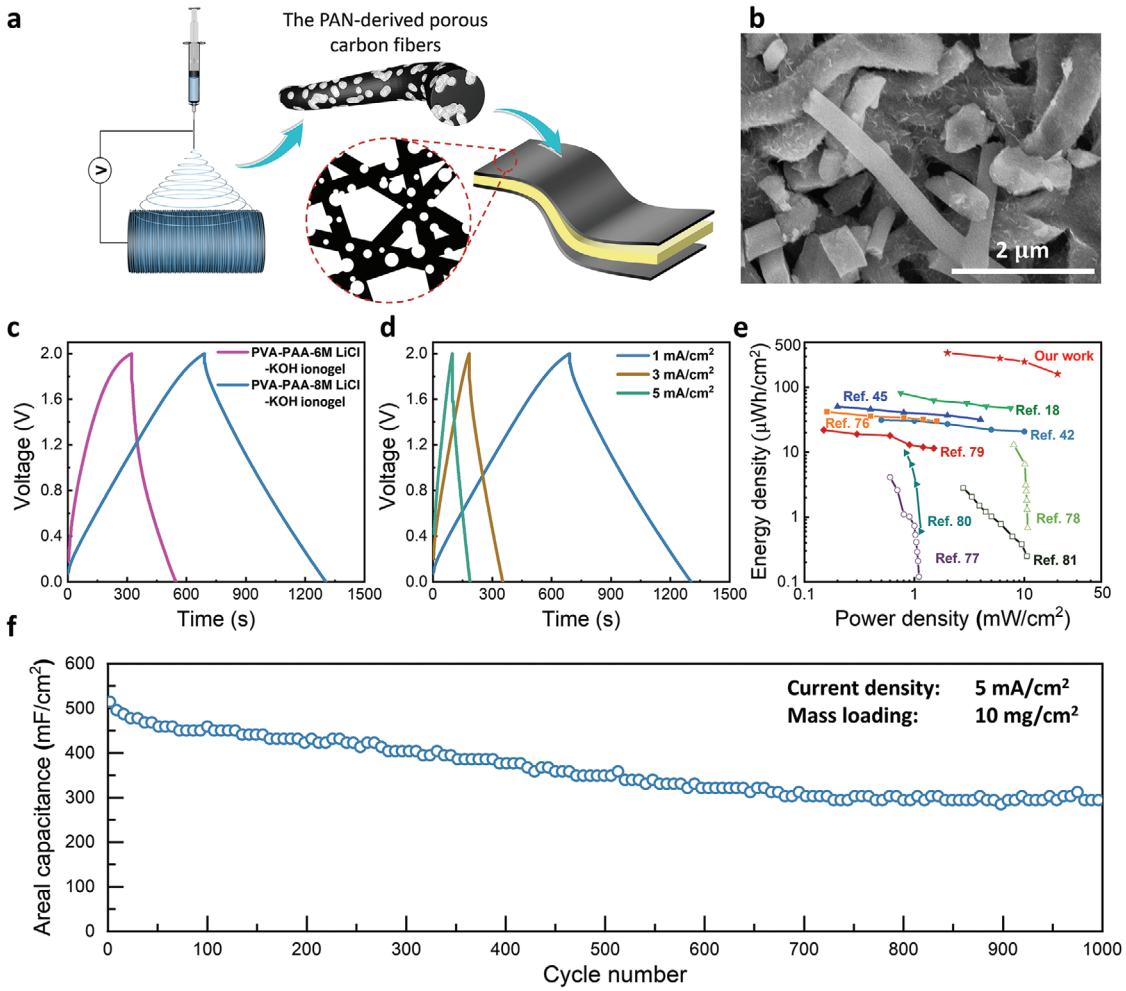

Figure 5. Schematic and electrochemical performance of the solid-state supercapacitor with the ionogel electrolyte and PAN-derived porous carbon fibers (PPCF) electrodes. a) Schematic. b) SEM image of the PPCF. Galvanostatic charge-discharge curves of gel-based supercapacitors c) with different ionogels and d) at various scan rates. e) Ragone plot comparison.[18,42,45,76–81] f) Cycling stability of the supercapacitor without sealing.

We attribute these behaviors in ionic conductivity to the time-varying gain or loss of water in different gels that affect their ion mobilities. Generally, a sufficient amount of water and adequate porosity of the polymer structure facilitate the ion transfer in a gel, since the low viscosity of water ensures ion mobility, and a high porous microstructure benefits the ionic liquid impregnation, and therefore, reduces the ion transfer tortuosity.[66] Comparing the initial three data points of the ionogel in both Figure 4a,b, we conclude that the initial increase of ionic conductivity is due to the slight water absorption of the ionogel from the atmosphere. This water absorption eventually reaches thermodynamic equilibrium after ≈2 h, given the low RH of 20%. By contrast, the water solvent in a hydrogel keeps evaporating due to the low humidity, hence reducing its ionic conductivity. The two hydrogels with LiCl (PVA-PAA-LiCl and PVA-PAA-LiCl-KOH) show a slower decrease of ionic conductivity over time for two reasons. First, it is known that LiCl greatly facilitates water retention in a hydrogel.[67] Second, the additional ions in these hydrogels potentially provide extra capabilities of ion transfer despite the water loss over time. This is further supported by the much slower decrease of ionic conductivity in the PVA-PAA-LiCl-KOH hydrogel. These explanations are also validated by the measured ionic conductivities in hydrogels and ionogels with various concentrations of LiCl. Meanwhile, the ionogel exhibits a satisfying ESW of 2.0 V (Figure S15, Supporting Information), which is moderate among other existing ionogels but much larger than that of hydrogels (Figure S16, Supporting Information).

Furthermore, the ionogel maintains good mechanical properties at low temperatures, with a stretchability of 9, strength of 0.6 MPa, and fracture toughness of 1612 J m^{-2} at −30 °C (Figure S17, Supporting Information). It is proud that the comprehensive performance of our product in terms of ionic conductivity and stretchability surpasses that of existing ionogels (Figure 4d), which has the potential to be employed as a promising GPE for wearable energy storage units.

To demonstrate its performance as a solid-state supercapacitor, the ionogel was sandwiched between two homemade electrospun polyacrylonitrile-derived porous carbon fibers (PPCF) electrodes (**Figure 5**a). The SEM images reveal that the as-spun PAN fibers are 300–700 nm in diameter (Figure S18, Supporting

Information). After KOH activation, a large number of tiny pores were created on the surface of carbon fibers (Figure 5b). These dense and tiny pores increase the specific surface area of the electrodes and allow more double-layer charge storage, enhancing the capacitance of the supercapacitor (Figure S19, Supporting Information).

The capacitance and coulombic efficiency of the supercapacitor were characterized by the use of galvanostatic charge–discharge (GCD). Figure 5c shows GCD curves of solid-state supercapacitors made of 6 and 8 M LiCl-treated ionogels at a scan rate of 1 mA cm^{-2}. Compared to the 6 M LiCl-treated supercapacitor, the 8 M LiCl-treated supercapacitor exhibits a smaller voltage drop (0.06 vs 0.22 V), a higher areal capacitance (615 vs 224 mF cm^{-2}), and a higher coulombic efficiency (93% vs 76%), since the 8 M LiCl-treated supercapacitor processes a lower equivalent series resistance and higher ionic conductivity. In addition, GCD curves of the 8 M LiCl-treated supercapacitor show a near-ideal triangular shape in Figure 5d, suggesting an excellent electric double-layer capacitance performance. This supercapacitor displays a high areal capacitance of 615 mF cm^{-2} at a scan rate of 1 mA cm^{-2}, superior to most reported gel-based solid-state supercapacitors (Figure S20, Supporting Information).[18,42,45,70,76,77] The outstanding areal capacitance of this solid-state supercapacitor benefits from the synergy of the high specific surface area of the PPCF electrode, the excellent ionic conductivity of the ionogel electrolyte, as well as low bulk resistance of the assembled solid-state supercapacitor (Figure S21, Supporting Information).

Moreover, this supercapacitor exhibited its ability to be applied at cold temperatures. As shown in Figure S22 (Supporting Information), the discharge time of the supercapacitor decreases with the reducing temperature, indicating a negative correlation between capacitance and temperature. This tendency agrees with the temperature dependency of ionic conductivity in ionogel, as aforementioned in Figure 4a. Surprisingly, the 8 M-supercapacitor delivered an areal capacitance of 110 mF cm^{-2} at a low temperature of −30 °C. Therefore, this ionogel is potentially applied to store energy in an extremely low temperature environment.

For the power and energy density, this ionogel-based supercapacitor also outperforms previous works (Figure 5e). The current supercapacitor shows a high energy density of 341.7 μWh cm^{-2} with a power density of 2.0 mW cm^{-2} at 1 mA cm^{-2}, and a high power density of 20 mW cm^{-2} with an energy density of 161 μWh cm^{-2} at 10 mA cm^{-2}. Furthermore, the cycling air stability of the solid-state supercapacitor is shown without any additional packaging or sealing. Despite little liquid loss and slight reactivity with airborne components at high voltages, the ionogel-based supercapacitor demonstrates reasonable stability, retaining 62% of its capacitance after 1000 cycles (Figure 5f).

3. Conclusion

In conclusion, we fabricated a novel ionogel with excellent electrochemical performance, mechanical properties, and physical stability through ion impregnation and solvent exchange. The ionogel shows a mechanical stretchability of 26, strength of 1.34 MPa, and fracture toughness of 4175 J m^{-2}, as well as self-strengthening with large mechanical hysteresis over 5000 cyclic loads. The reversible hydrogen bonds make the ionogel free from fatigue damage. Based on our understanding of the most up-to-date research, this ionogel demonstrates the highest room temperature ionic conductivity of 3.18 S m^{-1} among all reported ionogels, which remains exceptionally high at 0.48 S m^{-1} even at −30 °C. The ionogel is physically stable with 96% weight retention for 40 h at ambient temperature and 20% HR. To verify its potential for application in energy storage units, a solid-state supercapacitor was assembled using highly porous carbon fibers as electrodes and this highly ionic-conductive ionogel as the electrolyte. The supercapacitor delivers an aerial capacitance of 615 mF cm^{-2} at a current density of 1 mA cm^{-2}, a maximum energy density of 341.7 μWh cm^{-2} at 1 mA cm^{-2}, and a maximum power density of 20 mW cm^{-2} at 10 mA cm^{-2}. These performances surpass most reported gel-based solid-state supercapacitors, highlighting the promise of this ionogel. More significantly, the microstructures and ion concentrations elucidated by the comprehensive experimental investigation will guide future fine-tuning of ionogel's mechanical and electrochemical properties for diverse applications, including lightweight, high-performance, easy-carrying stretchable energy storage devices.

4. Experimental Section

Materials: Polyvinyl alcohol (PVA, hydrolyzed), 1-Ethyl-3-methylimidazolium ethyl sulfate ([EMIM][DCA]), acrylic acid (AA, anhydrous), lithium chloride (LiCl, anhydrous free-flow), potassium hydroxide (KOH), N, N-Dimethylformamide (DMF), and N-Methylpyrrolidone (NMP) were purchased from Fisher Scientific. The carbon conductive additive, Super P, was obtained from MTI Corporation. α-ketoglutaric acid (α-keto, 99.0% (T)), Polyacrylonitrile (PAN) with an average molecule weight of 15,000 g mol^{-1}, and poly(vinylidene fluoride) (PVDF) with an average molecule weight of 534,000 g mol^{-1} were purchased from Sigma–Aldrich. To form solutions, 8 g of PVA was dissolved into 92 g of deionization (DI) water at 90 °C for 3 h to produce an 8 wt% PVA solution, 1.2 g of PAN was dissolved into 8.8 g of DMF to produce a 12 wt% PAN solution, and 1 g of PVDF was dissolved into 9 g of NMP to produce a 10 wt% PVDF solution.

Synthesis of PVA-PAA Hydrogels: The prepared PVA solution (PVA 8 g, water 92 g) was cooled down to room temperature. Afterward, AA monomers of 72 g and α-ketoglutaric acid of 0.36 g (as photo-initiator, 0.5 wt% of AA monomers) were added into the solution. The solution was then mixed and vacuumed for 2.5 min to reach homogeneous and subsequently poured into glass modes of 5 × 1 × 0.1 cm^3, covered by a transparent glass sheet. Finally, the solution was polymerized under UV irradiation (365 nm, 30 W) overnight, leading to the PVA-PAA hydrogel.

Synthesis of PVA-PAA Ionogels: The synthesized PVA-PAA hydrogel was immersed in 100 mL of 6 or 8 M LiCl solution for 24 h. The resulting PVA-PAA-LiCl hydrogel was then immersed in saturated KOH solution for 1 h to form the PVA-PAA-LiCl-KOH hydrogel. Afterward, the surface of the hydrogel was gently washed with DI water to remove any residual KOH solution. The hydrogel was frozen in liquid nitrogen and placed in a freeze-dry machine (FreeZone 6, Labconco Corporation) for 36 h. Finally, the freeze-dried gel was immersed in the ionic liquid [EMIm][DCA] for 24 h to form the PVA-PAA-LiCl-KOH ionogel. To further show the advantage of the current method of solvent exchange with freeze-drying, Ionogels were synthesized from two control experiments: i) solvent exchange without freeze-drying: A PVA-PAA hydrogel was directly prepared, immersed the gel into an ionic liquid, and evaporated the water in the gel, and ii) one-pot polymerization: A gel was directly polymerized from a precursor solution containing PVA, AA monomers, water, and ionic liquid, and subsequently evaporated the water in the gel. Figure S23 (Supporting Information) shows the stress–stretch behaviors of the three gels, where the gel from the current method shows much higher strength and stretchability.

Polyacrylonitrile-Derived Porous Carbon Fibers (PPCF) Preparation: The preparation for the PPCF was based on the previous work.[82] Briefly, the prepared PAN solution was loaded into a syringe with a 27 gauge needle (inner diameter 0.21 mm, length 13 mm). Electrospinning was carried out at a voltage of 15 kV. PAN mesh was subjected to thermo-treatments, including stabilization, carbonization, and activation, to endow it with high conductivity and high porosity. All thermo-treatments were conducted in a tubular furnace (GSL 1600X, MTI Corporation). Specifically, the PAN mesh was first stabilized in the air at a heating rate of 1°C min^{-1} to 250 °C and held at 250 °C for 1 h. Afterward, the stabilized PAN nanofibers were stored in the furnace with a heating rate of 5°C min^{-1} to 1000 °C and carbonized in a nitrogen environment at 1000 °C for 1 h. To improve the porosity of PAN carbon fibers, solid KOH was ground with carbonized PAN fibers at a weight ratio of 3:1. The mixture was heated to 1000 °C with a heating rate of 5°C min^{-1} and kept in a furnace containing flowing N_2 for 1 h. Finally, samples were dialyzed in DI water to remove any residual KOH. The dialyzed-activated PPCF was lyophilized for utilization.

Solid-State Supercapacitor Assembly: A combination of 80 wt% PPCF, 10 wt% Super P, and 10 wt% PVDF was used to make the electrodes. The produced slurry was coated on aluminum foil (MTI Corporation) and dried at 80 °C for 12 h in an oven. To assemble a solid-state supercapacitor, free-standing PPCF electrodes were peeled off the aluminum foil and placed above and below the ionogel.

Materials Characterization: Morphologies of gels were characterized by SEM (Hitachi S4800) at 3 kV. Functional groups of gels were investigated by FTIR (Cary 630 FTIR, Agilent). TGA (TA Q50, Inc.) was conducted from room temperature to 600 °C with a heating rate of 2°C min^{-1} at a nitrogen atmosphere to study the thermal stability of gels.

Monotonic and Cyclic Tensile Tests: The monotonic and cyclic tensile tests were conducted using an Instron tensile tester (Instron 34TM-5). Samples of hydrogels and ionogels were cut into rectangular strips of 0.5 cm width and 0.08–0.12 cm thickness, and mounted into the tensile tester to form a gauge length of 4 cm. The nominal stress is defined as the measured force divided by the cross-sectional area of a sample in the reference (undeformed) state. The stretch was defined as the ratio between the deformed length and the original gauge length. For the uniaxial tensile test, the strain rate was set to 0.1 s^{-1}. For the cyclic tensile test, the strain rate was set to 0.33 s^{-1}. All mechanical tests were conducted at a room temperature of 20–22 °C.

Fracture Tests: The fracture toughness of a prepared gel was measured using the edge-crack test.[35] Specifically, a small crack of fixed length was initially precut in the middle of the sample edge, with the schematic shown in Figure S8a (Supporting Information). The precut sample has a rectangular shape of 5 mm width, 20 mm length, and 0.8-1.2 mm thickness, and 1 mm initial crack length. For the edge-crack test, the strain rate was set to 0.1 s^{-1}. All mechanical tests were conducted at a room temperature of 20–22 °C. The fracture toughness Γ is calculated as $\Gamma = (6/\sqrt{\lambda_c})cW(\lambda_c)$, where λ_c is the fracture stretch of the same sample without precut crack, c is the length of the precut crack, and $W(\lambda_c) = \int_1^{\lambda_c} s d\lambda$ is the work of rupture, calculated as the integral of the nominal stress–stretch (s–λ) curve of the uncut sample up to fracture. The stress-stretch curves of different gels with precut cracks are presented in Figure S8b (Supporting Information). To measure the fracture toughness at −30 °C, the cut and uncut samples were prepared first and subsequently frozen. Afterward, they were taken out and immediately tested on the Instron machine enclosed by a temperature chamber.

Electrochemistry Characterization: An electrochemical station (Biologic SP150) was applied to measure the ionic conductivity of gels. The low-temperature electrochemical performance was measured with the help of a temperature test chamber (VT 4002, AME Energy Co., Ltd.). A Biologic MPG-2 battery cycler was used to assess the cyclic voltammetry (CV) curves of ionogels in a range of 0–3 V (vs stainless steel), with a scan rate of 10 mV s^{-1} at room temperature. Galvanostatic charging–discharging was conducted in a range of 0–2 V, and cycling stability property was measured in a range of 0–1.8 V, both using an 8-channel tester (Wuhan LAND Electronic Co., Ltd.) at room temperature of 25 °C. The specific areal capacitance (C, mF cm^{-2}), energy density (E, mWh cm^{-2}), and powder density (P, mW cm^{-2}) of the supercapacitor were calculated using the following equations: $C = 2(It)/(VA)$, $E = 0.5CV^2/3600$, and $P = 3600E/t$, in which I, t, V, and A are the current (mA), discharge time (s), potential (V), and total area of electrodes (cm^2), respectively.[42] The capacitance of PPCF electrodes was measured in a two-electrode system beaker cell using 6 M KOH aqueous solvent electrolyte. The specific mass capacitance (C_m, F g^{-1}) of electrodes was calculated following the equation $C_m = 4It/(V \times m)$, where I, t, V, m are the current (A), discharge time (s), potential (V), and total mass (g) of electrodes, respectively.

Supporting Information

Supporting Information is available from the Wiley Online Library or from the author.

Acknowledgements

Y.W. and Z.W. contributed equally to this work. This work is supported by the startup funds of H.Z. and R.B. at Northeastern University, USA. The authors acknowledge the Northeastern University Center for Renewable Energy Technology (NUCRET) for the use of SEM.

Conflict of Interest

The authors declare no conflict of interest.

Data Availability Statement

Research data are not shared.

Keywords

ionic conductivity, ionogel, stretchability, supercapacitor, toughness

Received: August 15, 2023
Revised: November 17, 2023
Published online:

[1] K. Keum, J. W. Kim, S. Y. Hong, J. G. Son, S.-S. Lee, J. S. Ha, *Adv. Mater.* **2020**, *32*, 2002180.
[2] L. Li, Z. Lou, D. Chen, K. Jiang, W. Han, G. Shen, *Small* **2018**, *14*, 1702829.
[3] G. Shao, R. Yu, N. Chen, M. Ye, X. Y. Liu, *Small Methods* **2021**, *5*, 2000853.
[4] L. Li, L. Wang, T. Ye, H. Peng, Y. Zhang, *Small* **2021**, *17*, 2005015.
[5] L. Yue, J. Ma, J. Zhang, J. Zhao, S. Dong, Z. Liu, G. Cui, L. Chen, *Energy Storage Mater.* **2016**, *5*, 139.
[6] S. Alipoori, S. Mazinani, S. H. Aboutalebi, F. Sharif, *J. Energy Storage* **2020**, *27*, 101072.
[7] C. Keplinger, J.-Y. Sun, C. C. Foo, P. Rothemund, G. M. Whitesides, Z. Suo, *Science* **2013**, *341*, 984.
[8] J.-Y. Sun, X. Zhao, W. R. K. Illeperuma, O. Chaudhuri, K. H. Oh, D. J. Mooney, J. J. Vlassak, Z. Suo, *Nature* **2012**, *489*, 133.
[9] T. Binninger, A. Heinritz, R. Mohamed, *ChemRxiv* **2020.**
[10] C. Jiao, Q. Shao, M. Wu, B. Zheng, Z. Guo, J. Yi, J. Zhang, J. Lin, S. Wu, M. Dong, Z. Guo, *Polymer* **2020**, *190*, 122196.

[11] H. Gao, Z. Zhao, Y. Cai, J. Zhou, W. Hua, L. Chen, L. Wang, J. Zhang, D. Han, M. Liu, *Nat. Commun.* **2017**, *8*, 15911.
[12] L. Zhang, D. Jiang, T. Dong, R. Das, D. Pan, C. Sun, Z. Wu, Q. Zhang, C. Liu, Z. Guo, *Chem. Rec.* **2020**, *20*, 948.
[13] J. Feng, Y. Wang, Y. Xu, Y. Sun, Y. Tang, X. Yan, *Energy Environ. Sci.* **2021**, *14*, 2859.
[14] Y. Ding, J. Zhang, L. Chang, X. Zhang, H. Liu, L. Jiang, *Adv. Mater.* **2017**, *29*, 1704253.
[15] X. Liu, D. Wu, H. Wang, Q. Wang, *Adv. Mater.* **2014**, *26*, 4370.
[16] X. Yang, Y. Tian, B. Wu, W. Jia, C. Hou, Q. Zhang, Y. Li, H. Wang, *Energy Environ. Mater.* **2022**, *5*, 954.
[17] M. Wang, P. Zhang, M. Shamsi, J. L. Thelen, W. Qian, V. K. Truong, J. Ma, J. Hu, M. D. Dickey, *Nat. Mater.* **2022**, *21*, 359.
[18] Y. Shi, Y. Wang, Y. Gu, L. Zheng, S. Ma, X. Xu, *Chem. Eng. J.* **2020**, *392*, 123645.
[19] Y. Ge, X. Bu, L. Wang, L. Wu, X. Ma, W. Diao, D. Lu, *J. Appl. Polym. Sci.* **2021**, *138*, 50259.
[20] X. Zhao, J. Wu, Y. Zhou, Y. Pan, T. Lu, X. Song, J. Hu, *Extreme Mech. Lett.* **2021**, *46*, 101320.
[21] W. Chen, N. Li, Y. Ma, M. L. Minus, K. Benson, X. Lu, X. Wang, X. Ling, H. Zhu, *Biomacromolecules* **2019**, *20*, 4476.
[22] R. Marcombe, S. Cai, W. Hong, X. Zhao, Y. Lapusta, Z. Suo, *Soft Matter* **2010**, *6*, 784.
[23] C. Yang, Q. Wu, W. Xie, X. Zhang, A. Brozena, J. Zheng, M. N. Garaga, B. H. Ko, Y. Mao, S. He, Y. Gao, P. Wang, M. Tyagi, F. Jiao, R. Briber, P. Albertus, C. Wang, S. Greenbaum, Y.-Y. Hu, A. Isogai, M. Winter, K. Xu, Y. Qi, L. Hu, *Nature* **2021**, *598*, 590.
[24] R. Bai, J. Yang, X. P. Morelle, Z. Suo, *Macromol. Rapid Commun.* **2019**, *40*, 1800883.
[25] R. Bai, J. Yang, Z. Suo, *Eur. J. Mech.-A/Solids* **2019**, *74*, 337.
[26] X. Zhao, M. Wang, Y. Chen, Z. Chen, T. Suo, W. Qian, J. Hu, X. Song, W.-N. Mei, R. Sabirianov, *ACS Appl. Mater. Interfaces* **2019**, *11*, 19421.
[27] M. Sun, J. Qiu, S. Jin, W. Liu, E. Sakai, *Colloids Surf. A* **2020**, *607*, 125438.
[28] I. Manavi-Tehrani, M. Rabiee, M. Parviz, M. R. Tahriri, Z. Fahimi, in *Preparation, Characterization and Controlled Release Investigation of Biocompatible pH-Sensitive PVA/PAA Hydrogels*, Wiley, Hoboken, NJ **2010**, pp. 457–465.
[29] J. Qiao, J. Fu, R. Lin, J. Ma, J. Liu, *Polymer* **2010**, *51*, 4850.
[30] T. Swift, L. Swanson, M. Geoghegan, S. Rimmer, *Soft Matter* **2016**, *12*, 2542.
[31] J. Y. Chang, D. Godovsky, M. Han, C. Hassan, J. Kim, B. Lee, Y. Lee, N. Peppas, R. Quirk, T. Yoo, in *Biopolymers PVA Hydrogels Anionic Polymerisation Nanocomposites*, Springer, Berlin, Vol. *153*, **2000**.
[32] J. Li, Z. Suo, J. J. Vlassak, *J. Mater. Chem. B* **2014**, *2*, 6708.
[33] E. Zhang, R. Bai, X. P. Morelle, Z. Suo, *Soft Matter* **2018**, *14*, 3563.
[34] J. Kim, G. Zhang, M. Shi, Z. Suo, *Science* **2021**, *374*, 212.
[35] K. Mayumi, J. Guo, T. Narita, C. Y. Hui, C. Creton, *Extreme Mech. Lett.* **2016**, *6*, 52.
[36] R. Bai, Q. Yang, J. Tang, X. P. Morelle, J. Vlassak, Z. Suo, *Extreme Mech. Lett.* **2017**, *15*, 91.
[37] S. Lin, J. Liu, X. Liu, X. Zhao, *Proc. Natl. Acad. Sci. U. S. A.* **2019**, *116*, 10244.
[38] X. Liu, T.-C. Tang, E. Tham, H. Yuk, S. Lin, T. K. Lu, X. Zhao, *Proc. Natl. Acad. Sci. U. S. A.* **2017**, *114*, 2200.
[39] R. Bai, J. Yang, X. P. Morelle, C. Yang, Z. Suo, *ACS Macro Lett.* **2018**, *7*, 312.
[40] S. Lin, X. Liu, J. Liu, H. Yuk, H.-C. Loh, G. A. Parada, C. Settens, J. Song, A. Masic, G. H. McKinley, *Sci. Adv.* **2019**, *5*, eaau8528.
[41] M. Hua, S. Wu, Y. Ma, Y. Zhao, Z. Chen, I. Frenkel, J. Strzalka, H. Zhou, X. Zhu, X. He, *Nature* **2021**, *590*, 594.
[42] S. Wang, D. Zhang, X. He, J. Yuan, W. Que, Y. Yang, I. Protsak, X. Huang, C. Zhang, T. Lu, P. Pal, S. Liu, S. Y. Zheng, J. Yang, *Chem. Eng. J.* **2022**, *438*, 135607.
[43] Q. Zheng, X. Li, Q. Yang, C. Li, G. Liu, Y. Wang, P. Sun, H. Tian, C. Wang, X. Chen, J. Shao, *J. Power Sources* **2022**, *524*, 231102.
[44] J. Liu, H. Song, Z. Wang, J. Zhang, J. Zhang, X. Ba, *J. Mater. Sci.* **2020**, *55*, 3991.
[45] Z. Yong, S. Wang, X. Wang, G. Liu, D. Liang, Y. Cui, F. Liu, D. Wang, Z. Wang, *J. Alloys Compd.* **2022**, *893*, 162197.
[46] H. H. Rana, J. H. Park, G. S. Gund, H. S. Park, *Energy Storage Mater.* **2020**, *25*, 70.
[47] J. Wu, G. Xia, S. Li, L. Wang, J. Ma, *Ind. Eng. Chem. Res.* **2020**, *59*, 22509.
[48] A. Zhu, J. Huang, H. Xie, W. Yue, S. Qin, F. Zhang, Q. Xu, *Chem. Eng. J.* **2022**, *446*, 137032.
[49] X. Liu, O. O. Taiwo, C. Yin, M. Ouyang, R. Chowdhury, B. Wang, H. Wang, B. Wu, N. P. Brandon, Q. Wang, S. J. Cooper, *Adv. Sci.* **2019**, *6*, 1801337.
[50] J. Han, Y. Choi, J. Lee, S. Pyo, S. Jo, J. Yoo, *Chem. Eng. J.* **2021**, *416*, 129089.
[51] X. Liu, Z. Wen, D. Wu, H. Wang, J. Yang, Q. Wang, *J. Mater. Chem. A* **2014**, *2*, 11569.
[52] X. Liu, B. Wang, Z. Jin, H. Wang, Q. Wang, *J. Mater. Chem. A* **2015**, *3*, 15408.
[53] S. Guo, K. Zhao, Z. Feng, Y. Hou, H. Li, J. Zhao, Y. Tian, H. Song, *Appl. Surf. Sci.* **2018**, *455*, 599.
[54] X. Liu, B. Wu, N. Brandon, Q. Wang, *Energy Technol.* **2017**, *5*, 220.
[55] C. X. Xing, H. T. Zhang, S. S. Pan, M. Yao, B. S. Li, Y. Q. Zhang, S. J. Zhang, *Mater. Today Energy* **2020**, *18*, 100527.
[56] C. Yin, X. Liu, J. Wei, R. Tan, J. Zhou, M. Ouyang, H. Wang, S. J. Cooper, B. Wu, C. George, Q. Wang, *J. Mater. Chem. A* **2019**, *7*, 8826.
[57] D. Kim, P. K. Kannan, C.-H. Chung, *ChemistrySelect* **2018**, *3*, 2190.
[58] C. Lu, X. Chen, *Chem. Commun.* **2019**, *55*, 8470.
[59] H. Li, Z. Feng, K. Zhao, Z. Wang, J. Liu, J. Liu, H. Song, *Nanoscale* **2019**, *11*, 3689.
[60] Z. Wang, J. Liu, J. Zhang, S. Hao, X. Duan, H. Song, J. Zhang, *Cellulose* **2020**, *27*, 5121.
[61] H. H. Rana, J. H. Park, E. Ducrot, H. Park, M. Kota, T. H. Han, J. Y. Lee, J. Kim, J.-H. Kim, P. Howlett, M. Forsyth, D. Macfarlane, H. S. Park, *Energy Storage Mater.* **2019**, *19*, 197.
[62] C. Lu, X. Chen, *Chem. Phys. Lett.* **2020**, *755*, 137814.
[63] P. Flouda, D. Bukharina, K. J. Pierce, A. V. Stryutsky, V. V. Shevchenko, V. V. Tsukruk, *ACS Appl. Mater. Interfaces* **2022**, *14*, 27028.
[64] D. H. Cho, K. G. Cho, S. An, M. S. Kim, H. W. Oh, J. Yeo, W. C. Yoo, K. Hong, M. Kim, K. H. Lee, *Energy Storage Mater.* **2022**, *45*, 323.
[65] J. Lan, B. Zhou, C. Yin, L. Weng, W. Ni, L.-Y. Shi, *Polymer* **2021**, *231*, 124111.
[66] T.-T. Nguyen, A. Demortière, B. Fleutot, B. Delobel, C. Delacourt, S. J. Cooper, *npj Comput. Mater.* **2020**, *6*, 123.
[67] Y. Bai, B. Chen, F. Xiang, J. Zhou, H. Wang, Z. Suo, *Appl. Phys. Lett.* **2014**, *105*, 151903.
[68] S. I. Fletcher, F. B. Sillars, N. E. Hudson, P. J. Hall, *J. Chem. Eng. Data* **2010**, *55*, 778.
[69] J. Sun, Y. Yuan, G. Lu, L. Li, X. Zhu, J. Nie, *J. Mater. Chem. C* **2019**, *7*, 11244.
[70] Y. Zhai, W. Hou, M. Tao, Z. Wang, Z. Chen, Z. Zeng, X. Liang, P. Paoprasert, Y. Yang, N. Hu, S. Song, *Adv. Mater.* **2022**, *34*, 2205560.
[71] T. Guillemin, C. Douard, K. Robert, B. Asbani, C. Lethien, T. Brousse, J. Le Bideau, *Energy Storage Mater.* **2022**, *50*, 606.
[72] Y. Gao, G. Chen, X. Wang, H. Yang, Z. Wang, W. Lin, H. Xu, Y. Bai, C. Wu, *ACS Appl. Mater. Interfaces* **2020**, *12*, 22981.
[73] W. C. Poh, A. L.-S. Eh, W. Wu, X. Guo, P. S. Lee, *Adv. Mater.* **2022**, *34*, 2206952.
[74] Y. Wu, W. Jiang, X. Zhang, J. Wang, D. Chen, Y. Ma, W. Yang, *Macromol. Rapid Commun.* **2022**, *43*, 2200480.

[75] L. Negre, B. Daffos, V. Turq, P. L. Taberna, P. Simon, *Electrochim. Acta* **2016**, *206*, 490.
[76] S. Zheng, C. (J.) Zhang, F. Zhou, Y. Dong, X. Shi, V. Nicolosi, Z.-S. Wu, X. Bao, *J. Mater. Chem. A* **2019**, *7*, 9478.
[77] Y. Shi, Y. Zhang, L. Jia, Q. Zhang, X. Xu, *ACS Appl. Mater. Interfaces* **2018**, *10*, 36028.
[78] K. Wang, X. Zhang, C. Li, X. Sun, Q. Meng, Y. Ma, Z. Wei, *Adv. Mater.* **2015**, *27*, 7451.
[79] B. Asbani, B. Bounor, K. Robert, C. Douard, L. Athouël, C. Lethien, J. Le Bideau, T. Brousse, *J. Electrochem. Soc.* **2020**, *167*, 100551.
[80] C. Jin, H.-T. Wang, Y.-N. Liu, X.-H. Kang, P. Liu, J.-N. Zhang, L.-N. Jin, S.-W. Bian, Q. Zhu, *Electrochim. Acta* **2018**, *270*, 205.
[81] P. Pazhamalai, K. Krishnamoorthy, V. K. Mariappan, S. Sahoo, S. Manoharan, S.-J. Kim, *Adv. Mater. Interfaces* **2018**, *5*, 1800055.
[82] X. Sun, Q. Li, D. Cao, Y. Wang, A. Anderson, H. Zhu, *Small* **2022**, *18*, 2105678.